

Received by OSTI



Lawrence Berkeley Laboratory
UNIVERSITY OF CALIFORNIA

Materials & Chemical Sciences Division

National Center for Electron Microscopy

Presented at ISIAT '89, Tokyo, Japan, June 5-7, 1989

Fundamental Studies of Grain Boundary Structure and Properties in ICB Aluminum

K.H. Westmacott and U. Dahmen

May 1989



DISTRIBUTION OF THIS DOCUMENT IS UNLIMITED

Prepared for the U.S. Department of Energy under Contract Number DE-AC03-76SF00098

MASTER

DISCLAIMER

This report was prepared as an account of work sponsored by an agency of the United States Government. Neither the United States Government nor any agency thereof, nor any of their employees, makes any warranty, express or implied, or assumes any legal liability or responsibility for the accuracy, completeness, or usefulness of any information, apparatus, product, or process disclosed, or represents that its use would not infringe privately owned rights. Reference herein to any specific commercial product, process, or service by trade name, trademark, manufacturer, or otherwise does not necessarily constitute or imply its endorsement, recommendation, or favoring by the United States Government or any agency thereof. The views and opinions of authors expressed herein do not necessarily state or reflect those of the United States Government or any agency thereof.

DISCLAIMER

Portions of this document may be illegible in electronic image products. Images are produced from the best available original document.

FUNDAMENTAL STUDIES OF GRAIN BOUNDARY STRUCTURE AND
PROPERTIES IN ICB ALUMINUM

K.H. Westmacott and U. Dahmen

LBL--27187

National Center for Electron Microscopy
Materials and Chemical Sciences Division
Lawrence Berkeley Laboratory
1 Cyclotron Road, Berkeley, CA. 94720

DE89 014884

1. Introduction

Thin films prepared by the Ionized-Cluster-Beam (ICB) technique, pioneered at Kyoto University [1], are of great interest for both their fundamental structure and properties and their potential for practical applications. ICB research has burgeoned in the last few years with emphasis concentrated on understanding the physics of the deposition process, determining the size and structure of clusters, correlating structure and properties, exploring the range of materials that can be prepared by the technique, and some initial attempts at using the films in electronic device applications [2]. At Berkeley a research program has been initiated, in collaboration with Professor Yamada and his colleagues at Kyoto University, to investigate a different aspect of ICB films. We are exploiting the unique bicrystal microstructure that forms with some thin film/substrate combinations to conduct a fundamental investigation of grain boundary structure and properties.

Initially, the studies are being carried out on aluminum bicrystal films formed by deposition on a {100} silicon single crystal substrate. Two types of transmission electron microscopy (TEM) experiments will be reported. The changes in microstructure that occur during in-situ heating are followed in a high voltage electron microscope (HVEM) equipped with a heating stage and video camera. High resolution imaging of specific grain boundary segments is performed on a second HVEM capable of resolving the position of atom columns in the core regions of a grain boundary. Complementary information obtained by the two techniques is helping us to understand the structure and properties of grain boundaries as well as learn more about ICB thin films.

In the final section of this paper, the results of preliminary high-resolution observations of silver clusters dispersed on a carbon grid are given.

2. Experimental

Specimens for the electron microscopy were made from samples of ICB deposited aluminum on {100} silicon prepared at the Kyoto Ion-Beam Engineering Laboratory, by well established procedures. Discs 3mm in diameter were trepanned from the substrate taking care to protect the thin Al deposited film from damage. The discs were then back-thinned to electron transparency from the silicon side using either a silicon chemical polish followed by brief ion beam cleaning, or by mechanical dimpling followed by more extensive ion-beam thinning. The thickness of the Al deposited film in the present work was 125nm. With the preparation technique used, the TEM specimen consisted of the free standing ICB Al (wedge-shaped in cross section) near the hole at the center of the disc. Further away from the hole the Al remained supported by the silicon substrate (see Fig. 1).

High resolution images of grain boundaries were obtained in thin regions of the Al marked 1 in Fig. 1. The JEOL 1000 Atomic Resolution Microscope with a point resolution of 0.16nm operated at 800 kV was used for this purpose.

In-situ studies were performed on the Kratos EM 1500 operated at 1500 kV in thicker regions of the foil, marked 2 and 3. This microscope is equipped with a lens-coupled 80mm, low light level, high-resolution Westinghouse TV camera used with a YAG scintillator, and a double tilt, 750°C side entry heating rod. A few additional high resolution, in-situ heating experiments were conducted on the Stanford Philips 430 electron microscope equipped with a super-twin lens and single-tilt heating stage [3].

Image-processing was used to enhance the high resolution images of discrete clusters to discriminate them from the amorphous carbon substrate on which they were deposited.

3. Experimental Results

3.1. Review of ICB Aluminum Microstructure

The unique bicrystal structure of ICB aluminum films deposited on a {100} silicon substrate is now well established [1,4,5,6,7]. Figure 2c is a conventional TEM micrograph illustrating the typical microstructure of a film in the as-deposited condition. It shows a fine grain structure which on closer examination is seen to consist of individual grains deposited in a bicrystal arrangement. This is confirmed in Fig. 2a which is a selected area diffraction pattern from a $20 \mu\text{m}^2$ region of the aluminum showing two types of grains are present, both with a {110} plane parallel to the {100} surface of the substrate but rotated with respect to each other by 90° about the normal to substrate

surface. One of the 110 patterns in Figure 2a is marked with dots to distinguish it from the other. Figure 2b is a similar pattern taken from a region where the Al is backed by the substrate. Strong 220 and 400 reflections from the silicon are now also present together with many additional spots arising from double-diffraction between the Al and Si.

Analysis of this pattern reveals the origin of the bicrystal structure. The [100] direction in the [011] zone of the Al aligns itself, with equal probability, with the [110], or [1-10] direction in the {001} silicon substrate. This is illustrated schematically in Fig. 3. The accurate alignment, $100_{Al} \parallel 110_{Si}$, is possibly due to a match in the respective planar spacings, i.e. $d_{(100)Al} = 4.05 \text{ \AA}$, $d_{(110)Si} = 3.84 \text{ \AA}$; $\Delta d/d = 5 \%$

3.2. Annealed Microstructures

During post-deposition annealing of specimens, coarsening of the Al bicrystal structure occurs, grain boundaries reduce their area (and hence energy) by rotating normal to the film surface, and individual grains develop pronounced facets. The latter two effects are what make annealed ICB Al films ideal specimens for high resolution studies of grain boundary structure. Since each grain is rotated 90° relative to its neighbor, all the boundaries are of the same type ($90^\circ <110>$ tilt) and the atomic structure, particularly at facets, can be readily observed as a function of boundary orientation.

To investigate the changes in microstructure that occur during annealing, heat treatments were performed in-situ.

3.3. In-Situ Annealing Studies

Attention was focused on three aspects of the film annealing behavior: 1) overall changes in microstructure, 2) a comparison of the structure of the supported and unsupported films, 3) facet development and disappearance.

Figure 4a-c are micrographs comparing the structure before (a) and after annealing at $\sim 640^\circ\text{C}$ for the unsupported (b) and silicon supported film (c). The annealing process was observed on the TV monitor during heating and following attainment of the selected temperature.

The severe foil bending that occurs during heating or cooling originates from the different expansion coefficients for the Si and Al, $\alpha \approx 5 \times 10^{-6} \text{ K}^{-1}$ and $24 \times 10^{-6} \text{ K}^{-1}$ respectively. Over a 600 K temperature range strains of magnitude $\epsilon = \Delta\alpha\Delta T \approx 10^{-2}$ develop, which is well in excess of the yield strain for Al ($\sim 10^{-3}$). This has been confirmed

by careful measurements of the change in curvature of a SiO_2/Si substrate coated with Al during a heating/cooling cycle [8].

Further confirmation that plastic deformation of the Al occurs is provided by the observation that high concentrations of slip traces are observed in the Al backed by Si following a heating/cooling cycle.

Despite the foil buckling, it was possible to make observations on microstructural changes that occur during heating. It was apparent that the occasional dislocation within a grain annealed out, the average grain size increased, the film became much flatter - suggesting elastic stresses had been relieved - and faceting of the grain boundaries occurred in the temperature range 200-250°C.

From a comparison of Figs. 4 (b) and (c) it is evident that the average grain size is markedly greater for the supported Al than for the unsupported regions of the film. From a limited analysis a factor of 5 difference was estimated. This is an interesting effect that warrants further study. However, it is uncertain to what extent extraneous deformation may have played a role in the process.

To study the process of facet development in more detail the specimen was cycled several times between 200 and 640°C. Observation of many different grains during this treatment confirmed that grains developed pronounced facets during the cooling stage of the cycle to 200°C and, conversely, developed more curvature during the heating to 640°C (see Fig. 5). Most of the facets are related by angles of 45°, which is consistent with the expected presence of symmetric and asymmetric boundaries, but other subsidiary facets are also present (see, for example, Fig. 5 b,d,e). These preliminary results suggest that with further study it will be possible to rank the grain boundary orientations in order of their relative energies.

3.4. High Resolution Studies

In order to obtain detailed information on interface structure the grains of a bicrystal must be oriented so that both have a low index zone axis, as well as the common interface between them, accurately parallel to the electron beam. ICB Al deposited on {100} silicon provide excellent specimens for the study of grain boundary atomic structure at high resolution [9]. Since all grains in the ICB Al have a common $\langle 110 \rangle$ direction perpendicular to the film surface, those boundaries which have rotated into orientations normal to the film surface are suitable for study.

From analysis of the diffraction patterns, and direct high resolution imaging of grains in annealed specimens, it is shown that faceting occurs predominantly on those planes that are parallel to the mirror planes of the Si substrate, i.e. the planes marked by white lines in the bicrystal diffraction pattern in Fig. 2b. The vertical and horizontal planes form the symmetrical $\langle 110 \rangle$ tilt boundary shown in Fig. 6a while the diagonal planes in Fig. 2b form the asymmetrical boundary shown in Fig. 6b. The two types of facets make an angle of 45° with each other, and thus the shape of sharply faceted grains is that of a truncated square.

The two high resolution images reveal interesting detail of the boundary structure at the atomic level. While the symmetrical boundary in Fig. 6a exhibits a clear periodicity, but deviates fractionally from the 90° misorientation, the asymmetrical boundary in Fig. 6b has no periodicity but clearly shows the precise 90° misorientation of the two grains, since $\{001\}$ planes in one grain are conjugated to $\{011\}$ planes in the other grain. In both boundaries atomic relaxations are confined to a relatively small region in the vicinity of the boundary. Atomistic calculations of the grain boundary structure, currently underway, will help to understand the precise local atomic arrangements and rigid body shifts measurable from such high resolution images.

A common geometrical model for the description of bicrystal structures is the coincidence site lattice (CSL). A 90° $\langle 110 \rangle$ misorientation does not produce a rational CSL. It can, however, be approximated with arbitrary accuracy by nearly rational CSL's. A Σ_{17} $\langle 110 \rangle$ CSL forms at misorientations of 86.6° and 93.4° , i.e. at $\pm 3.4^\circ$ from the precise 90° misorientation. Successively closer approximations are obtained at Σ_{99} ($\pm 0.6^\circ$ from 90°), Σ_{577} ($\pm 0.1^\circ$ from 90°), etc. However, as the accuracy of the misorientation angle increases, the physical significance of the CSL description looses its meaning since for Σ_{577} only one in 577 atoms is in coincidence position. For that reason, usually only boundaries with $\Sigma < 50$ are considered. But precise measurement of the misorientation, and the periodicity in the boundary have shown that Fig 6a is a symmetrical Σ_{99} $\langle 110 \rangle$ tilt boundary on a $\{557\}$ plane. Since this is an exact measurement it follows that the 90° misorientation has been locally adjusted by 0.6° to allow a high- Σ periodic boundary to form. In contrast, Fig. 6b shows a boundary that has maintained the precise 90° misorientation but without periodicity. Other examples have been found where a local deviation allowed a Σ_{17} boundary to form. To understand how such local orientation changes are accomplished and how they are related to facets and local boundary structure is the subject of ongoing investigation. It is anticipated that in-situ TEM studies of boundary behavior at temperatures where boundary migration can occur,

will provide clues on important phenomena such as faceting, orientation changes, phase transformations in the boundary and boundary reconstruction.

3.5. Dynamic In-Situ High Resolution Studies

In addition to studying the static structure of grain boundaries it is of fundamental interest to investigate the dynamic properties about which very little is presently known.

Some preliminary high-resolution observations of boundary migration were carried out using the Stanford Philips EM430.

Thin regions of a specimen where the unsupported Al contained a boundary were examined at various temperatures up to $\sim 640^{\circ}\text{C}$. Once the temperature stabilized, relatively clear images could be recorded which, with the aid of image processing, are permitting mechanisms of boundary migration to be deduced. Figure 7 shows a typical sequence of time-averaged TV frames that were recorded as a boundary was in motion.

3.6. Imaging of Individual Clusters

High resolution TEM also provides a valuable tool for examining the morphology and structure of individual metal clusters [10]. For this purpose, an amorphous carbon-coated specimen grid was used as the substrate. Because of the small cluster size, the particles in the as-recorded film image are barely discernable (Fig. 8a). However, by digitizing and processing, the image of the metal cluster can be significantly enhanced relative to that of the substrate as seen in the examples of Fig. 8 b, c, and d. A variation in the cluster size and shape is found and the substructure varies from being single crystalline (b) to more complex particles with a preferred orientation (c), (d). It is probable that the complex particles are in fact multiple clusters and these are present on the substrate in much greater concentrations than the single clusters.

4. Conclusions

The Ionized-Cluster Beam technique offers an intriguing new method for preparing material ideally suited for study by high resolution TEM techniques. By virtue of its unique bicrystal structure and large number of grain boundaries present with a fixed misorientation, fundamental studies on boundaries in Al (deposited on $\{100\}$ Si), are now being conducted.

Initial work has focused on determining the atomic structure in the boundary as a function of boundary orientation, understanding boundary migration at the atomic level, studying the process and energetics of faceting, and characterizing the structure of individual clusters.

5. Acknowledgements

The authors are grateful to Professor I. Yamada and Dr. H. Usui for donating the samples and for stimulating discussions. We also appreciate Professor R. Sinclair's kind offer of use of the Stanford facilities, Alan Schwartzman's help with the experiments conducted there, and John Turner's help with the image processing. This work was supported by the Director, Office of Energy Research, Office of Basic Energy Sciences of the U.S. Department of Energy under contract #DE-AC03-76SF00098.

6. References

1. I. Yamada, H. Inokawa, and T. Takagi, *J. Appl. Phys.*, **56**, 2746 (1984).
2. Proc. Int'l Workshop on ICBT, ed. T. Takagi, Kyoto University, (1986).
3. R. Sinclair, T. Yamashita, M.A. Parker, K.B. Kim, K. Holloway and A.F. Schwartzman, *Acta Cryst.*, **A44**, 965 (1988).
4. M. Asano, S. Tanaka, H. Usui, I. Yamada and T. Takagi, Proc. 11th Symp. on ISIAT '87, Tokyo (1987), 337
5. M.C. Madden and B.M. Tracy, Proc. 45th Ann. Meeting of EMSA, G. W. Bailey, ed., San Francisco Press, 362 (1987).
6. U. Dahmen and K.H. Westmacott, *Scripta Metall.*, **22**, 1673 (1988).
7. U. Dahmen, K.H. Westmacott, I. Yamada, and M.C. Madden, Scanning 89/EM West, Long Beach, CA. April, 1989.
8. M.F. Doener, D.S. Gardner and W.D. Nix, *J. of Mat. Res.*, **1**, 845 (1986); P.A. Flinn, D.S. Gardner and W.D. Nix, *IEEE Trans. Electron Devices*, **ED-34**, 689 (1989).
9. U. Dahmen, J. Douin, C.J.D. Hetherington and K.H. Westmacott, MRS Symp. on High Resolution Microsc. of Materials, Boston, MA (1988).
10. H. Usui, M. Tanaka, I. Yamada, and T. Takagi, 7th Int'l. Conf. on Ion Implantation Techn. (1988); also Ref. 4, p. 133.

Figure Captions

Figure 1: Schematic diagram showing cross-section of TEM specimen and indicating regions where various observations were made.

Figure 2: Diffraction patterns from Al bicrystal (a), bicrystal and Si substrate (b), and conventional TEM micrograph of as-deposited ICB Al on {100} Si (c) .

Figure 3: Schematic diagram illustrating the relationships between the orientation of the Al bicrystal films and Si substrate.

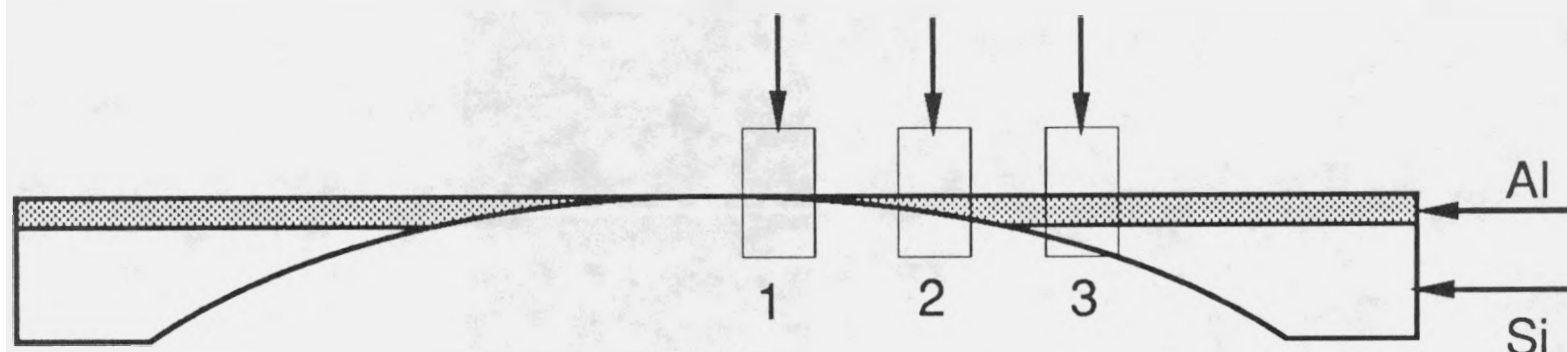
Figure 4: Series of micrographs showing the effects of in-situ annealing at 640°C; (a) as-deposited, (b) unsupported Al after annealing, (c) Al supported by the Si substrate after annealing. Note the factor of four change in magnification between (b) and (c).

Figure 5: Series of micrographs illustrating the reversible changes in shape of an Al grain (unsupported) during a thermal cycle between 20 and 640°C: (a) 100°C, (b) 250°C, (c) 640°C, (d) 200°C. Figures (a)-(d) are taken from a video tape; (e) is a film exposure of a different grain taken after the sample had been heated to 300°C.

Figure 6: High resolution micrographs showing the $\Sigma 99$ boundary structure for a symmetric boundary (a) and the structure of an asymmetric boundary (b). (courtesy MRS [9], micrographs by C.J.D. Hetherington)

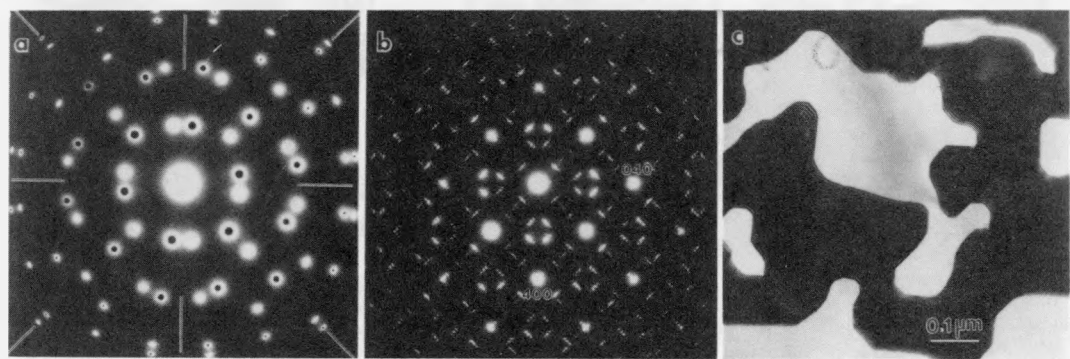
Figure 7. Series of high resolution images from video frames illustrating the lateral movement of a grain boundary by ledge propagation (see arrows) during in-situ heating.

Figure 8: High resolution micrographs of individual Ag clusters deposited on a carbon substrate. An as-recorded image is shown in (a), and computer enhanced images in (b), (c) and (d). The same cluster is seen as-recorded in (a) and Fourier filtered in (b).



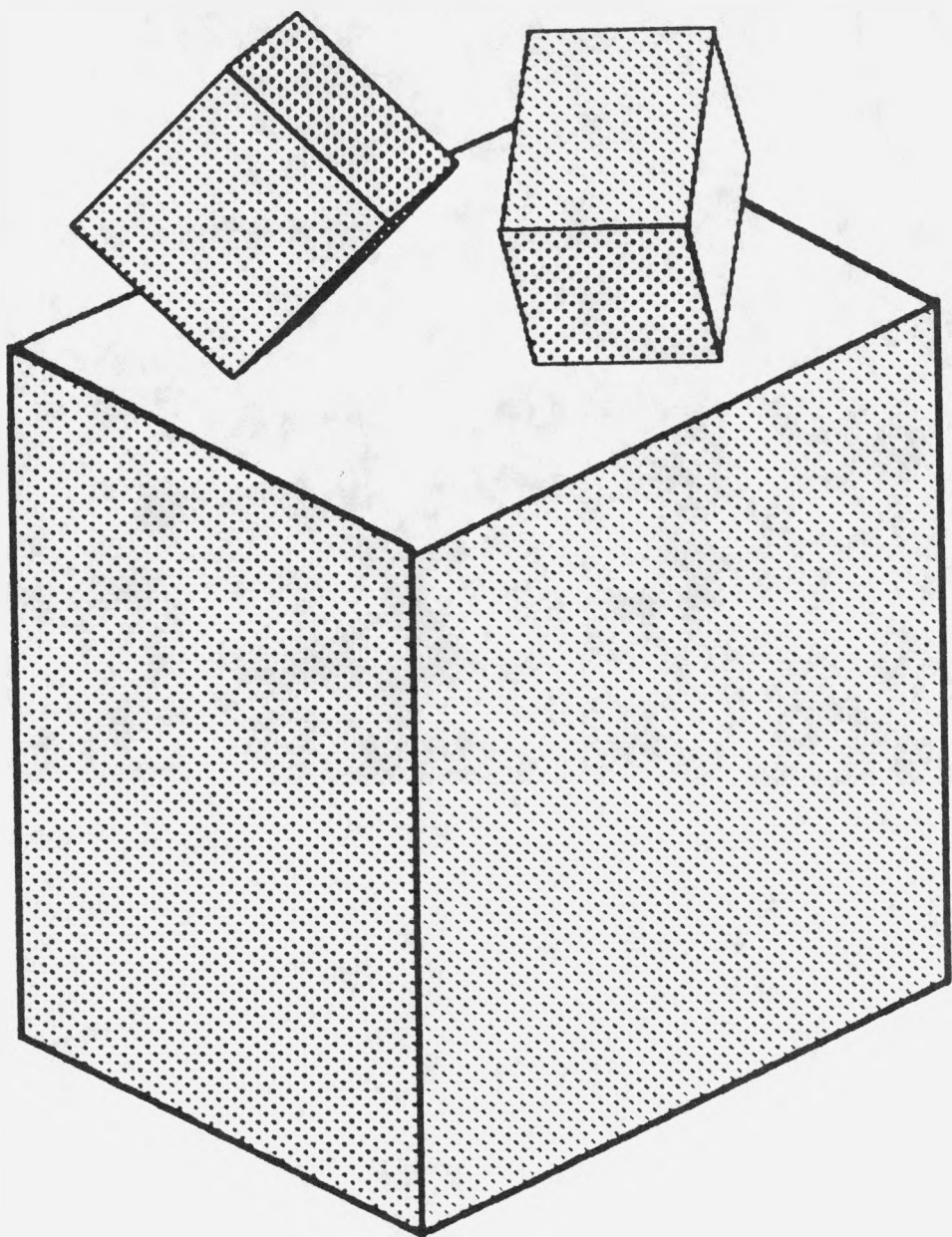
XBL 895-1862

Figure 1



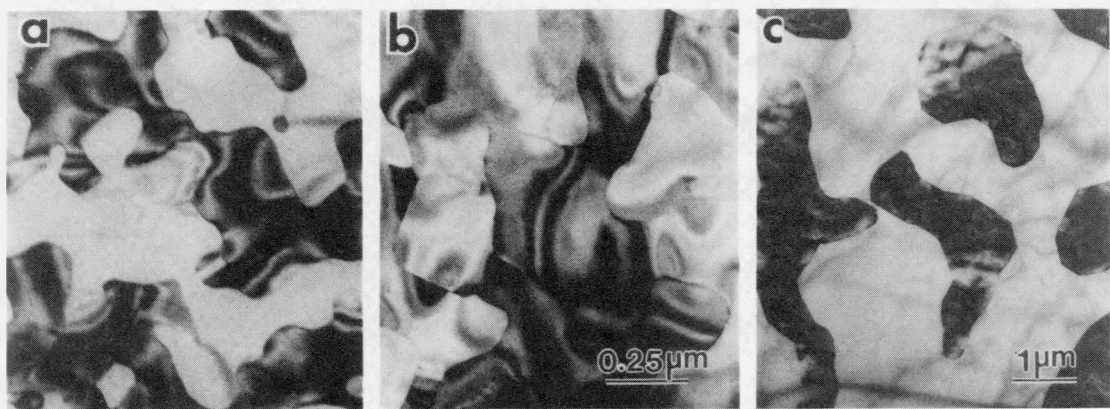
XBB 880-10322A

Figure 2



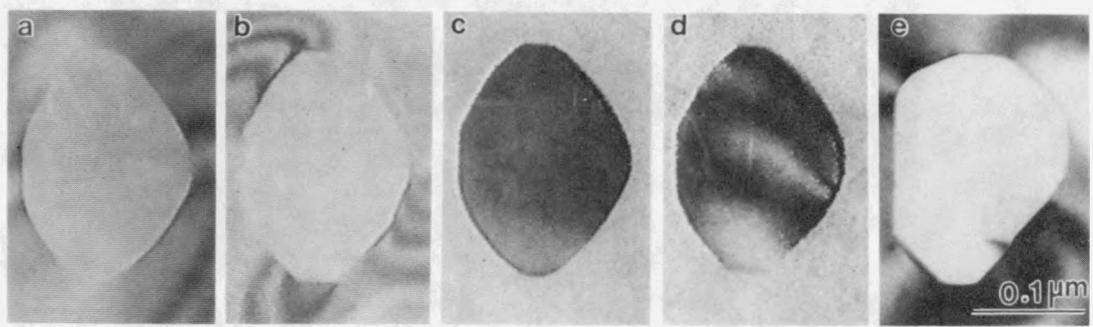
XBL 895-1863

Figure 3



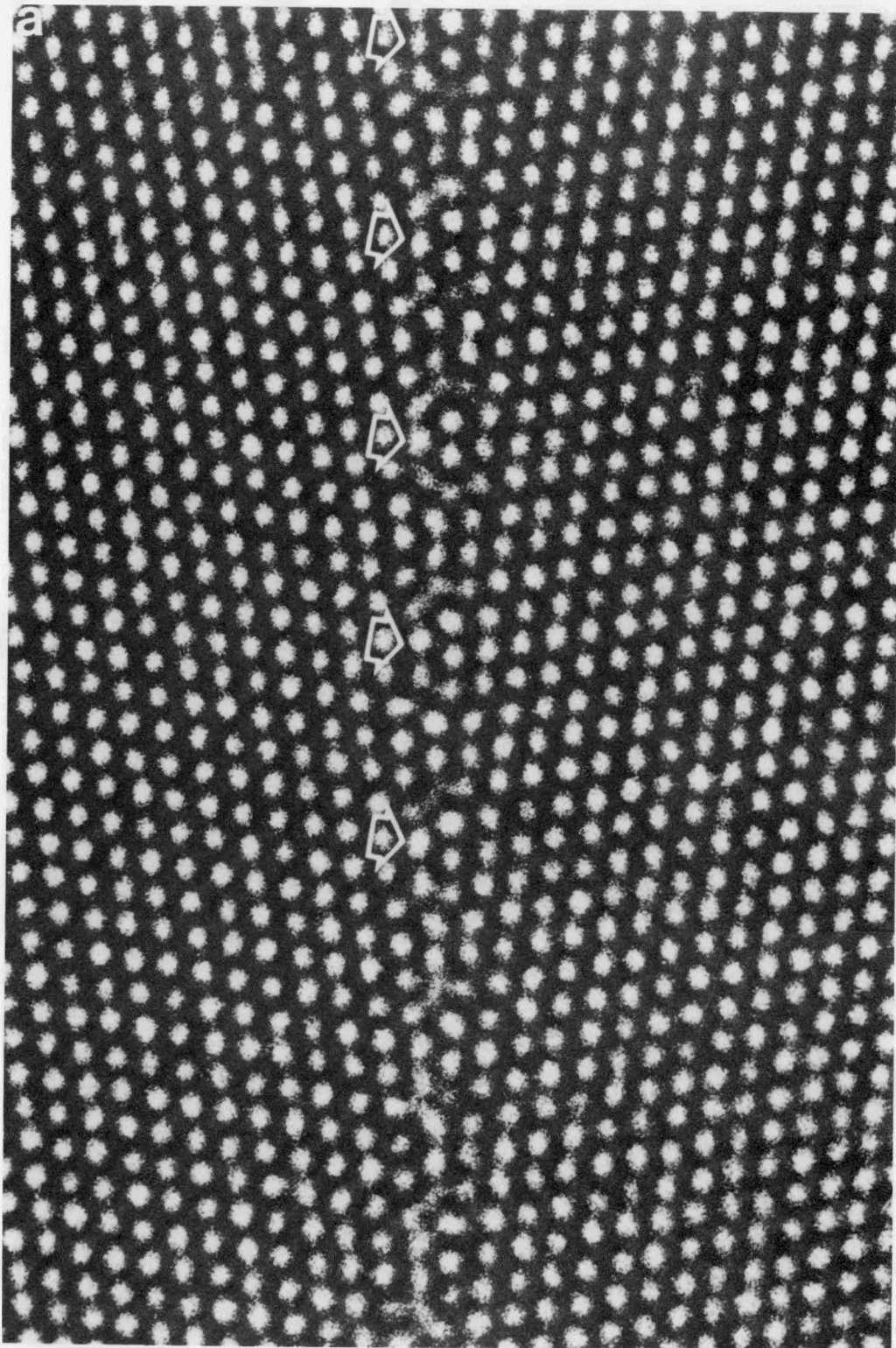
XBB 895-4010

Figure 4



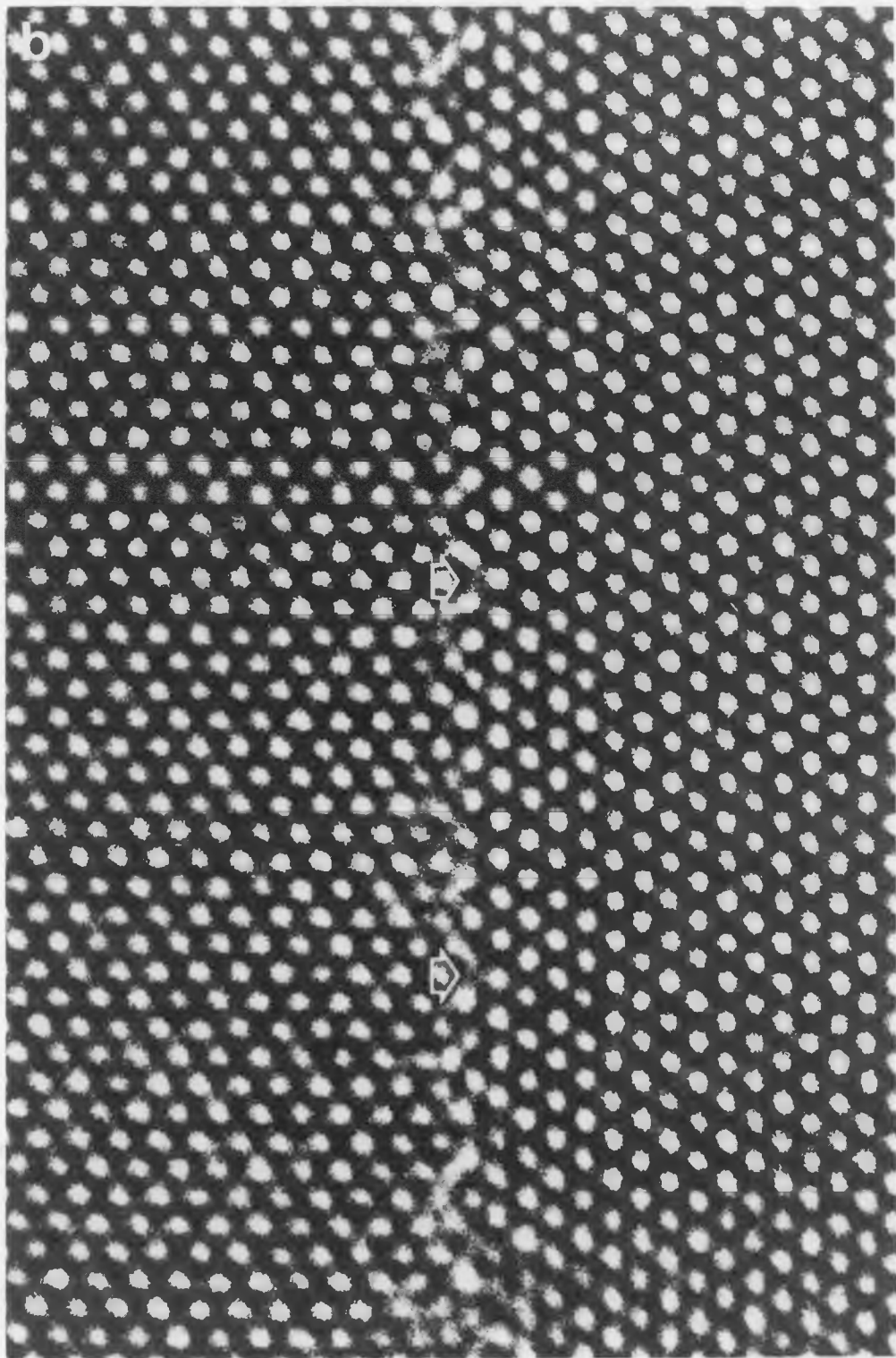
XBB 895-4011

Figure 5



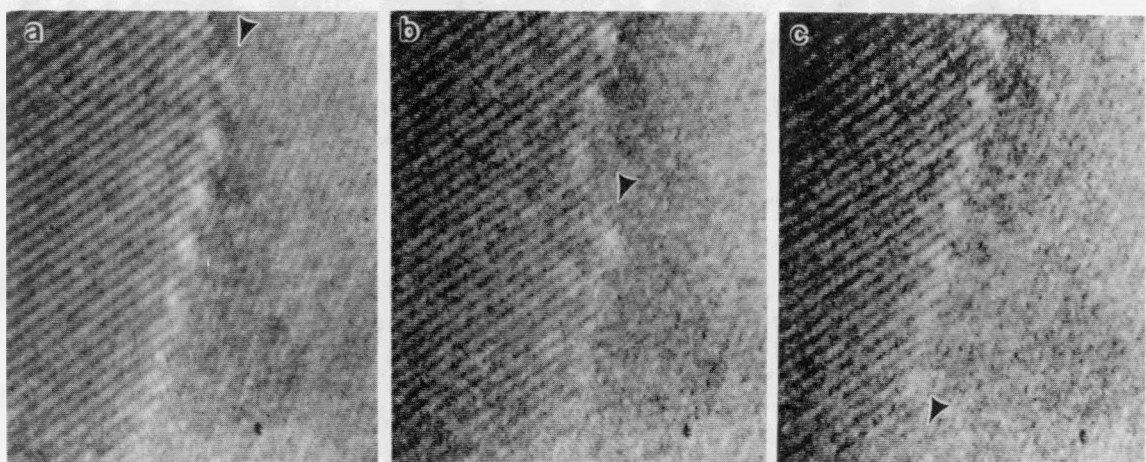
XBB 880-10320

Figure 6a



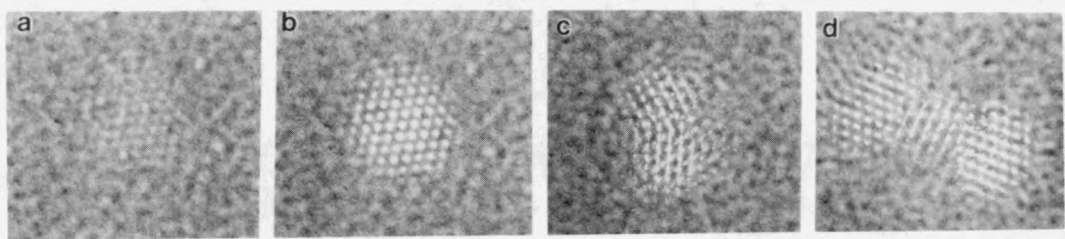
XBB 880-10319

Figure 6b



XBB 895-4009

Figure 7



XBB 895-4012

Figure 8